

# SURFACE ROUGHNESS AND NANOFLUID CONCENTRATION EFFECTS ON THE SURFACE WETTABILITY AND NANOFLUID BOILING HEAT TRANSFER

Leonardo Lachi Manetti, leomanetti@hotmail.com

Igor Seicho Kiyomura, igorseicho@gmail.com

Alex Pereira da Cunha, eng.alexpcunha@gmail.com

Marco Antonio de S. Peloso Junior, marcospeloso@gmail.com

\*Elaine Maria Cardoso, elainemaria@dem.feis.unesp.br (\*corresponding author)

UNESP – São Paulo State University, Department of Mechanical Engineering, Av. Brasil, 56, 15385-000, Ilha Solteira, SP, Brazil.

**Abstract.** *The fluid/surface interaction has an important influence on pool boiling phenomena and can be large affected by changing the surface roughness or the working fluid properties. This paper mainly focuses on the effect of surface roughness and nanofluid concentration on the wettability and also, on the heat transfer coefficient (HTC). In order to analyze the interaction between the surface roughness and nanoparticles deposited on the heating surface, the tests were performed on copper heating surfaces with different roughness values. The nanostructured surfaces were produced by maghemite and alumina nanoparticle deposition, for different mass concentration, via nanofluid boiling process. All surfaces were submitted to metallographic, roughness and wettability analysis. The roughness of nanocoated surface is a function of the boiled nanofluid concentration. As the nanofluid concentration increases the surface roughness increases and the contact angle decreases, characterizing a hydrophilic behavior. Concerning the heat transfer coefficient, it was observed that the smooth surface has the lowest values compared to the other samples. The porous nanolayer formed on the rough surfaces increases the thermal resistance of the surface, degrading the heat transfer; for smooth surfaces, the nanoparticle deposition increases the microcavities, increasing the boiling heat transfer. However, this enhancement only occurred for low nanofluid concentrations, for which the thermal conductivity of the nanofluid overcomes the thermal resistance of the nanolayer formed on the surface.*

**Keywords:** *pool boiling, heat transfer coefficient, nanofluid, wettability.*

## 1. INTRODUCTION

The application of nucleate pool boiling is common in many systems that need to dissipate high heat fluxes, such as nuclear reactors, macro and microelectronics, refrigeration and air-conditioner, among others. There are many variables that influence the boiling heat transfer, such as, the thermophysical properties of the working fluid and the heating surface morphology (Carey, 1992). In the last decades, researchers have been trying to develop more efficient heat transfer fluids to improve process efficiency and reduce operational costs. This is where nanofluids could play a key role, because they could potentially increase the boiling heat transfer.

The use of nanofluids on nucleate pool boiling have been extensively investigated because of their high thermal conductivity as well as the nanoscale structures deposited on the heating surface. However, the influence of nanofluid on the boiling heat transfer coefficient (HTC) has not been fully comprehended. Weng and Ding (2005), Soltani *et al.* (2009), Ahmed and Hamed (2012) e Wen (2012) reported a HTC enhancement of 30% to 40% as compared to pure water case. Moreover, Harish *et al.* (2011) found an increase of 90% in the HTC for Al<sub>2</sub>O<sub>3</sub>-water nanofluid as compared with pure water tests. In contrast, HTC deterioration were reported by Das *et al.* (2003), Bang and Chang (2005), Kim *et al.* (2007), Kwark *et al.* (2010), Shahmoradi *et al.* (2013) and Sarafraz and Hormozi (2014).

The differences on the HTC behavior occur mainly due the nanoparticle deposition on the heating surface. Narayan *et al.* (2007) introduce a surface-interaction parameter (SIP), which is the ratio between the average surface roughness,  $R_a$ , and the average diameter of the nanoparticle,  $d_p$ . According to the authors, when  $SIP > 1$ , the HTC increases due to the nanoparticles deposition in the cavities splitting a single active cavity into multiple ones. The Narayan parameter was used by other authors (Harish *et al.*, 2011; Raveshi *et al.* 2013), and it proved to be a suitable parameter to predicting the interaction between heating surface roughness and deposition of nanoparticles.

Others researches indicate that low nanofluids concentrations, lower than 0.01 vol.%, promote the boiling heat transfer. According to them, nanoparticle deposition occurs at a slower rate and the effect of the thermal conductivity of the nanofluid is more dominant than the effect of the nanoparticle deposition on the surface (Ahmed and Hamed, 2012; Shahmoradi *et al.*, 2013). For high nanofluids concentrations, the nanoparticle deposition occurs at a higher rate leading to a decrease in the number of active nucleation sites and an increase in the thermal resistance on the heating surface (Vafaei, 2015). Additionally, the nanoparticle deposition on the heating surface can increase the surface wettability reducing the nucleation sites density and degrading the HTC (Sarafraz *et al.*, 2016).

The aim of this work is to analyze the effect of the surface roughness and nanofluid concentration on the surface wettability, as well as the effects on the HTC behavior.

## 2. MATERIALS AND METHODS

### 2.1 Test surfaces preparation

The tests were performed on copper heating surfaces with different roughness values, corresponding to a smooth surface ( $R_a = 0.05 \mu\text{m}$ , namely SS) and a rough surface ( $R_a = 0.23 \mu\text{m}$ , namely RS). Prior to the pool boiling tests, all surfaces were cleaned with acetone.

Ten different copper surfaces, eight of them being nano-coated, were analyzed. These surfaces consisted of one smooth surface (SS); one rough surface (RS); four smooth surfaces with nanoparticle deposition, at low and high concentration of  $\text{Fe}_2\text{O}_3$ -water or  $\text{Al}_2\text{O}_3$ -water nanofluid (namely Fe-SS-LC, Fe-SS-HC, Al-SS-LC, and Al-SS-HC) and four rough surfaces with nanoparticle deposition, at low and high concentration of  $\text{Fe}_2\text{O}_3$ -water or  $\text{Al}_2\text{O}_3$ -water nanofluid (namely Fe-RS-LC, Fe-RS-HC, Al-RS-LC and Al-RS-HC). The nano-coated surfaces were obtained by the boiling process, applying a heat flux range of 100 to 800  $\text{kW/m}^2$ , of  $\text{Fe}_2\text{O}_3$ -water or  $\text{Al}_2\text{O}_3$ -water nanofluid. In order to verify the influence of nanolayer thickness on the surface roughness and wettability, two different nanofluid concentrations, 0.029 g/l (corresponding to low nanofluid concentration) and of 0.29 g/l (corresponding to high nanofluid concentration), were used.

The  $\text{Fe}_2\text{O}_3$ -water based nanofluid, with an average particle size of 10 nm, was synthesized following Massart's method (1982), in which  $\text{Fe}_2^+$  and  $\text{Fe}_3^+$  salts are precipitated in an alkaline medium and then dispersed in water. The  $\text{Al}_2\text{O}_3$ -water based nanofluid, with an average particle size of 10 nm, was prepared by the two-step method that involves generating nanoparticles and subsequently dispersing them into deionized water.

### 2.2 Pool boiling setup

The boiling chamber (Fig. 1) consists of a cube of 5 mm thick glass walls and overall dimensions 170 x 170 x 180 mm, which involves a borosilicate tube of internal diameter 90 mm, height 180 mm, and wall thickness 10 mm.

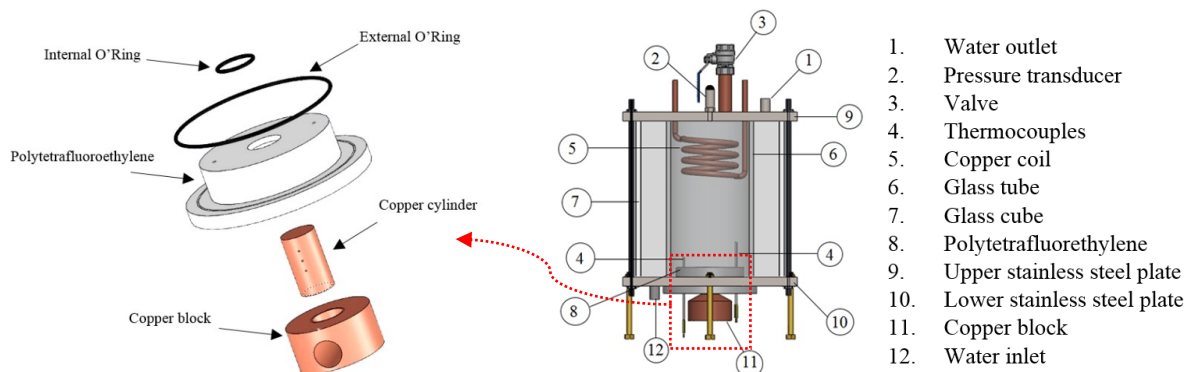


Figure 1. Pool boiling apparatus.

The test section consists of a copper block (20 mm diameter) with three K-type thermocouples fixed in the cylindrical part to determine the wall temperatures and the heat flux. The copper block is heated by one cartridge resistance with a maximum power of 300 W. The thermal insulation of the test section consists of polytetrafluoroethylene and vermiculite.

The temperature readings were acquired from the thermocouples by the data acquisition system Agilent 34970A. The heat transfer coefficient was calculated using the Newton's law of cooling given by

$$h = \frac{q''}{T_w - T_{sat}(p_{atm})} \quad (1)$$

where  $T_w$  is the measured temperature, and  $T_{sat}(p_{atm})$  corresponds to the saturation temperature of the water at atmospheric pressure

In order to ensure the steady state regime was achieved, each test had a duration of 1350 s for each applied heat flux, but only the temperature data for the last 500 s (corresponding to 100 experimental data points) of the test interval were considered. The temperature uncertainty was  $\pm 0.4 \text{ }^\circ\text{C}$ . For all surfaces tested, the experimental uncertainty for the heat flux and for the heat transfer coefficient varied from 15.0 % to 1.7 %, and from 17.5 % to 3.1 % respectively.

### 2.3 Surface characterization techniques

Different techniques were used to obtain the surfaces characteristics, prior and after each test:

- Structural and chemical information by scanning electron microscopy (SEM), performed by the EVO LS15 Zeiss® scanning electron microscope;
- Average surface roughness ( $R_a$ ), with the same scanning area for all surfaces, by a Mitutoyo Surftest SJ 301 model;
- Static contact angles measure by analysis of pictures of a sessile droplet (20  $\mu$ l of deionized water, Fe<sub>2</sub>O<sub>3</sub>-water or Al<sub>2</sub>O<sub>3</sub>-water nanofluid) using an experimental apparatus showed in Fig. 2.

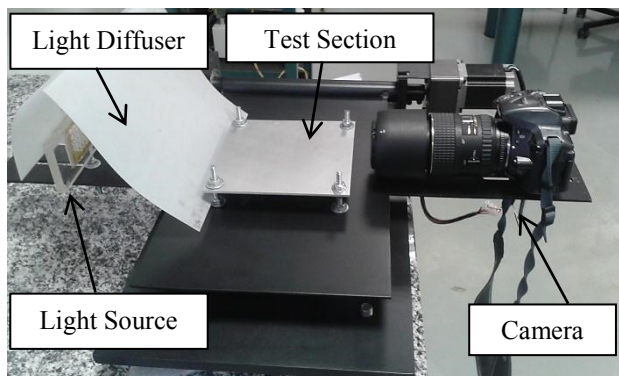


Figure 2. Experimental apparatus to measure the contact angle.

The apparatus to measure the static contact angle consists of a test surface, a camera, a green LED light source, a light diffuser and an aluminum plate where the test surface is fixed. The measurements were made for two different randomly selected locations on the surfaces. The pictures were analyzed using image post processing software to shape the deionized water droplet.

The calibration process, based on that developed by Netto et. al. (2013) and by Kiyomura et. al. (2015) was validated by comparison with known angles. Semispherical bodies namely A, B and C made of glass were used, with shapes similar to the 2D image of the droplet positioned on the surface as one may observe in Fig. 3.

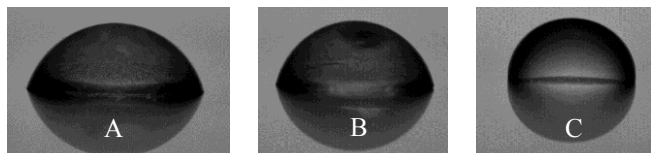


Figure 3. Semi-spherical proof bodies used to validate the contact angle measurements.

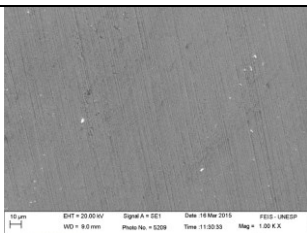
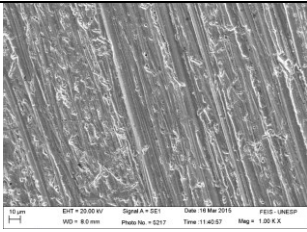
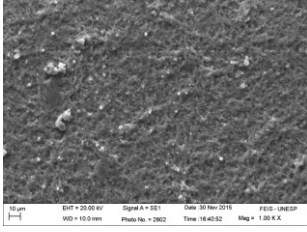
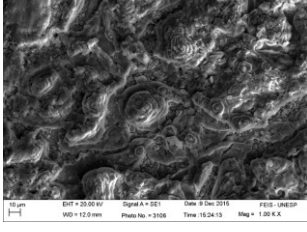
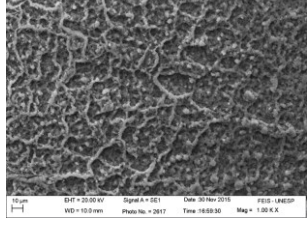
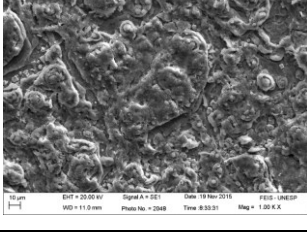
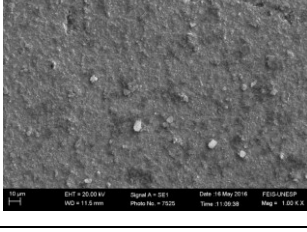
Three distinct operators analyzed each image and measured its contact angle by using image post processing software. Table 1 compares the contact angle based on the measurements and the respective estimated value from geometrical relations. The mean absolute error (MAE) value confirms that this method of picture analysis of a sessile droplet is accurate.

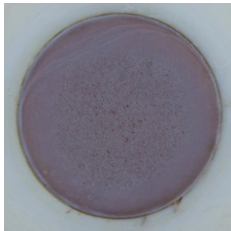
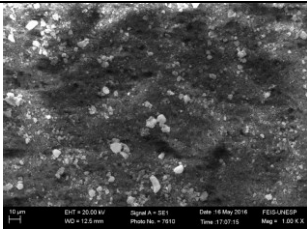
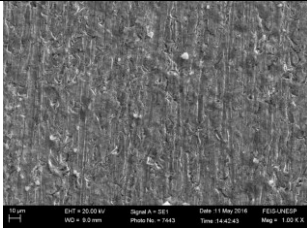
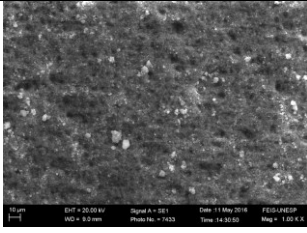
Table 1. Results of the contact angle measured on three semi-spherical proof bodies simulating droplets.

	<b>Proof body A</b>	<b>Proof body B</b>	<b>Proof body C</b>
<b>Operator 1</b>	76.90	81.56	93.92
<b>Operator 2</b>	74.69	80.68	94.86
<b>Operator 3</b>	76.45	80.50	94.51
$MAE = \frac{1}{N} \sum_{i=1}^N \left  \frac{\theta_{calc} - \theta_{exp}}{\theta_{calc}} \right $	1.04%	0.97%	0.47%

In the Table 2, one may observe the different copper surfaces tested in the present study and the respective metallographic analysis.

Table 2. Metallographic analysis for all surfaces tested in the present study.

Surface	SEM	EDS										
SS		<table border="1"> <thead> <tr> <th>Element</th> <th>Weight%</th> </tr> </thead> <tbody> <tr> <td>C</td> <td>2.94</td> </tr> <tr> <td>O</td> <td>1.77</td> </tr> <tr> <td>Al</td> <td>0.69</td> </tr> <tr> <td>Cu</td> <td>94.60</td> </tr> </tbody> </table>	Element	Weight%	C	2.94	O	1.77	Al	0.69	Cu	94.60
Element	Weight%											
C	2.94											
O	1.77											
Al	0.69											
Cu	94.60											
RS		<table border="1"> <thead> <tr> <th>Element</th> <th>Weight%</th> </tr> </thead> <tbody> <tr> <td>C</td> <td>4.43</td> </tr> <tr> <td>O</td> <td>1.67</td> </tr> <tr> <td>Al</td> <td>0.52</td> </tr> <tr> <td>Cu</td> <td>93.37</td> </tr> </tbody> </table>	Element	Weight%	C	4.43	O	1.67	Al	0.52	Cu	93.37
Element	Weight%											
C	4.43											
O	1.67											
Al	0.52											
Cu	93.37											
Fe-SS-LC		<table border="1"> <thead> <tr> <th>Element</th> <th>Weight%</th> </tr> </thead> <tbody> <tr> <td>O</td> <td>32.85</td> </tr> <tr> <td>Fe</td> <td>53.32</td> </tr> <tr> <td>Cu</td> <td>13.83</td> </tr> </tbody> </table>	Element	Weight%	O	32.85	Fe	53.32	Cu	13.83		
Element	Weight%											
O	32.85											
Fe	53.32											
Cu	13.83											
Fe-SS-HC		<table border="1"> <thead> <tr> <th>Element</th> <th>Weight%</th> </tr> </thead> <tbody> <tr> <td>C</td> <td>4.40</td> </tr> <tr> <td>O</td> <td>31.99</td> </tr> <tr> <td>Fe</td> <td>55.23</td> </tr> <tr> <td>Cu</td> <td>8.38</td> </tr> </tbody> </table>	Element	Weight%	C	4.40	O	31.99	Fe	55.23	Cu	8.38
Element	Weight%											
C	4.40											
O	31.99											
Fe	55.23											
Cu	8.38											
Fe-RS-LC		<table border="1"> <thead> <tr> <th>Element</th> <th>Weight%</th> </tr> </thead> <tbody> <tr> <td>O</td> <td>32.33</td> </tr> <tr> <td>Fe</td> <td>45.22</td> </tr> <tr> <td>Cu</td> <td>22.45</td> </tr> </tbody> </table>	Element	Weight%	O	32.33	Fe	45.22	Cu	22.45		
Element	Weight%											
O	32.33											
Fe	45.22											
Cu	22.45											
Fe-RS-HC		<table border="1"> <thead> <tr> <th>Element</th> <th>Weight%</th> </tr> </thead> <tbody> <tr> <td>C</td> <td>4.00</td> </tr> <tr> <td>O</td> <td>32.09</td> </tr> <tr> <td>Fe</td> <td>52.19</td> </tr> <tr> <td>Cu</td> <td>11.72</td> </tr> </tbody> </table>	Element	Weight%	C	4.00	O	32.09	Fe	52.19	Cu	11.72
Element	Weight%											
C	4.00											
O	32.09											
Fe	52.19											
Cu	11.72											
Al-SS-LC		<table border="1"> <thead> <tr> <th>Element</th> <th>Weight%</th> </tr> </thead> <tbody> <tr> <td>O</td> <td>26.14</td> </tr> <tr> <td>Al</td> <td>10.78</td> </tr> <tr> <td>Cu</td> <td>63.08</td> </tr> </tbody> </table>	Element	Weight%	O	26.14	Al	10.78	Cu	63.08		
Element	Weight%											
O	26.14											
Al	10.78											
Cu	63.08											

Al-SS-HC			<table border="1"> <thead> <tr> <th>Element</th> <th>Weight%</th> </tr> </thead> <tbody> <tr> <td>O</td> <td>61.27</td> </tr> <tr> <td>Al</td> <td>37.29</td> </tr> <tr> <td>Cu</td> <td>1.44</td> </tr> </tbody> </table>	Element	Weight%	O	61.27	Al	37.29	Cu	1.44
Element	Weight%										
O	61.27										
Al	37.29										
Cu	1.44										
Al-RS-LC			<table border="1"> <thead> <tr> <th>Element</th> <th>Weight%</th> </tr> </thead> <tbody> <tr> <td>O</td> <td>19.94</td> </tr> <tr> <td>Al</td> <td>9.01</td> </tr> <tr> <td>Cu</td> <td>71.05</td> </tr> </tbody> </table>	Element	Weight%	O	19.94	Al	9.01	Cu	71.05
Element	Weight%										
O	19.94										
Al	9.01										
Cu	71.05										
Al-RS-HC			<table border="1"> <thead> <tr> <th>Element</th> <th>Weight%</th> </tr> </thead> <tbody> <tr> <td>O</td> <td>60.80</td> </tr> <tr> <td>Al</td> <td>37.62</td> </tr> <tr> <td>Cu</td> <td>1.58</td> </tr> </tbody> </table>	Element	Weight%	O	60.80	Al	37.62	Cu	1.58
Element	Weight%										
O	60.80										
Al	37.62										
Cu	1.58										

### 3. RESULTS AND DISCUSSION

The experimental results showed that the enhancement or deterioration of nanofluids boiling heat transfer is strongly affected by the relative size between nanoparticles and heating surface morphology, and the interactions between them. In Figure 4, one may observe the boiling HTC curves for pure water as compared to the Fe<sub>2</sub>O<sub>3</sub>-water and Al<sub>2</sub>O<sub>3</sub>-water nanofluids, for different surfaces roughness and nanofluids concentrations.

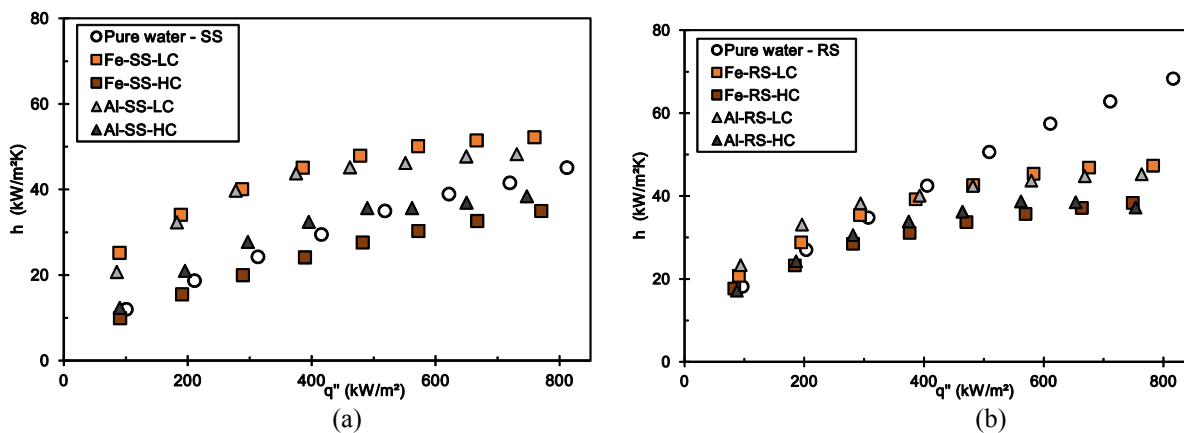


Figure 4. Boiling HTC curves for pure water, Fe<sub>2</sub>O<sub>3</sub>-water and Al<sub>2</sub>O<sub>3</sub>-water nanofluids. (a) smooth surface. (b) rough surface.

The nanoparticles deposition occurred for all surfaces tested, being more pronounced for high heat fluxes (higher than 400 kW/m<sup>2</sup>). The nanoparticles deposition not only increases the surface roughness but also changes the surface wettability. In Figure 5a, it is shown the surface roughness  $R_a$  before and after nanofluid boiling process against nanofluid concentration, for rough and smooth surface and for Fe<sub>2</sub>O<sub>3</sub>-water and Al<sub>2</sub>O<sub>3</sub>-water nanofluids. Similarly, in Figure 5b, it is shown the pure water static contact angles for each surface against the nanofluids concentration.

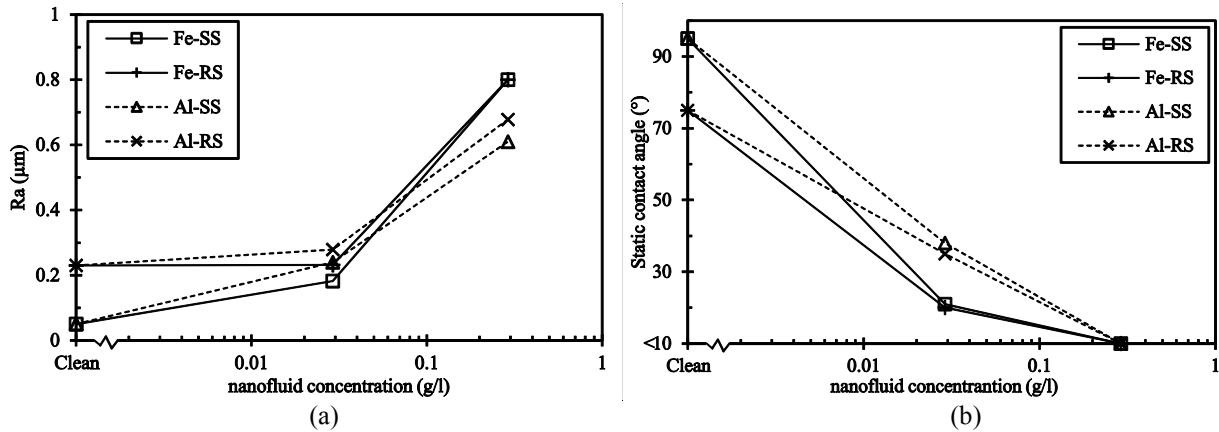


Figure 5. Heating surface behavior before and after nanofluid boiling process for different nanofluid concentrations. (a) surface roughness. (b) pure water static contact angles.

Figure 6 shows the static contact angle measurement for clean rough and smooth surfaces using pure water droplet, and also, Fe<sub>2</sub>O<sub>3</sub>-water and Al<sub>2</sub>O<sub>3</sub>-water nanofluids droplet.

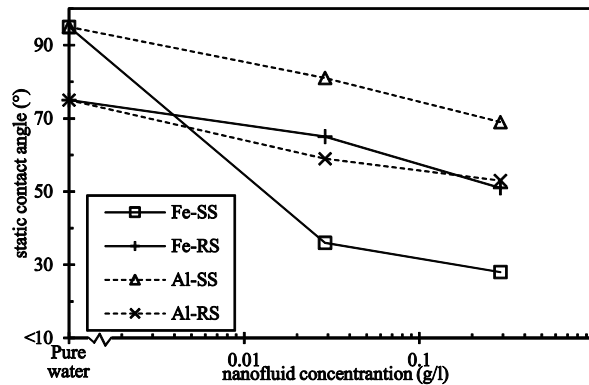


Figure 6. Static contact angle for clean rough and smooth surfaces using Fe<sub>2</sub>O<sub>3</sub>-water and Al<sub>2</sub>O<sub>3</sub>-water nanofluids droplet.

As can be seen in Fig. 6, both nanofluids increase the surface wettability due the change on the surface tension, caused by adding nanoparticles on the base fluid (Bhuiyan *et al.*, 2015). However, the wettability enhancement is more pronounced on the nanocoated surfaces, produced by the nanofluids boiling process (Fig. 5b). Also, the nanolayer formed on the heating surface increases the average roughness surface.

The surface roughness and the static contact angle depend on the working nanofluid and the nanofluid concentration. As nanofluid concentration increases the surface roughness, wettability and nanolayer thickness also increase.

Other researchers also reported changes in the heating surfaces after nanofluid boiling process, such as static contact angle reduction and surface roughness enhancement (Giljean *et al.*, 2011, Gu *et al.*, 2014, Cieśliński *et al.*, 2014). According to Zhang and Jacobi (2015), there is a relationship between the bubble nucleation sites and the nanoparticle deposition process, and also, the surface roughness and the static contact angle is a function of the original surface characteristics. In contrast to Zhang and Jacobi (2015), in the present work the original surface characteristics have less influence on the wettability behavior than the nanofluid concentration.

Regarding to heat transfer performance, the HTC for rough surface and for Fe<sub>2</sub>O<sub>3</sub>-water and Al<sub>2</sub>O<sub>3</sub>-water nanofluids has no change up to the 300 kW/m<sup>2</sup> as compared to pure water (Fig. 4b). For high heat fluxes values, it was observed deterioration in the HTC as compared to the pure water boiling curve. This could be explained by the decrease in the nucleation site density and, consequently, in the bubble frequency and its departure diameter, since the nucleation sites are filled by the nanoparticles and the static contact angle decreases. Moreover, as the nanofluid concentration increases the nanolayer formed on the heating surface also increases, leading to an enhancement in the thermal resistance and degradation in the HTC.

For smooth surfaces and for low nanofluid concentration (Fig. 4a), it was observed an increase in the boiling heat transfer for both Fe<sub>2</sub>O<sub>3</sub>-water and Al<sub>2</sub>O<sub>3</sub>-water nanofluid. This behavior is mainly due to the increase in the surface roughness by splitting a single nucleation site into multiple ones, leading to the enhancement in the HTC. It agrees with Narayan *et al.* (2007), who reported an enhancement in the HTC when SIP > 1. The nanofluid thermal conductivity can also play a role to increase the HTC, since the nanoparticles dispersed in the base fluid increase its thermophysical

properties. Also in Fig. 5a, as the nanofluid concentration increases the thermal resistance due to the nanoparticle deposition on heating surface overlaps the surface roughness enhancement, thus deteriorating the HTC for both working nanofluids.

#### 4. CONCLUSIONS

An analysis on the effect of nanofluid concentration and the surface roughness on the wettability and on the HTC was carried out. A metallographic, roughness and wettability characterization, before and after the nanofluid pool boiling tests was presented. The main results are:

- ✓ The nanofluids decrease the static contact angle, and this behavior is more pronounced on the nanocoated surfaces, produced by the nanofluids boiling process.
- ✓ The surface roughness and the static contact angle depend on the working nanofluid and the nanofluid concentration. As nanofluid concentration increases the surface roughness, wettability and nanolayer thickness also increase. In the present work, the original surface characteristics had less influence on the wettability behavior than the nanofluid concentration.
- ✓ For smooth surfaces and for low nanofluids concentration it was observed an enhancement in the HTC as compared to pure water, which is related to the increase in the nucleation sites density, due to changes in the surface morphology during nanofluid pool boiling. For rough surfaces and for low nanofluids concentrations, the HTC decreased mainly due to the decrease in the nucleation site density, since the nucleation sites are filled by the nanoparticles.
- ✓ Boiling heat transfer degradation was observed for high nanofluid concentration independently of the surface roughness. The thicker porous nanolayer formed on the heating surfaces increases the thermal resistance of the surface, degrading the HTC.

#### 5. ACKNOWLEDGEMENTS

The authors are grateful for the financial support from the PPGEM – UNESP/FEIS, from the National Council of Technological and Scientific Development of Brazil (CNPq grant number 458702/2014-5) and from FAPESP (grants numbers 2013/15431-7, 2014/07949-9, 2014/19497-5 e 2015/04025-3). The authors also extend their gratitude to Mrs. Maria de Fátima da Silva and Mr. Marcelo Parise from NFA/Instituto de Física - UNB for supplying the nanofluids.

#### 6. REFERENCES

- Ahmed, O. and Hamed, M. S., 2012. "Experimental investigation of the effect of particle deposition on pool boiling of nanofluids". *International Journal of Heat and Mass Transfer*, Vol. 55, No. 13, pp. 3423-3436.
- Bang, I. C. and Chang, S. H., 2005. "Boiling heat transfer performance and phenomena of Al<sub>2</sub>O<sub>3</sub>-water nano-fluids from a plain surface in a pool". *International Journal of Heat and Mass Transfer*, Vol. 48, No. 12, pp. 2407-2419.
- Bhuiyan, M.H.U., Saidur, R., Amalina, M.A., Mostafizur, R.M., Islam, AKMS., 2015. "Effect of nanoparticles concentration and their sizes on surface tension of nanofluids". *Procedia Engineering*, Vol. 105, pp. 431-437.
- Carey, V. P., 1992. *Liquid-vapor phase-change phenomena: an introduction to the thermophysics of vaporization and condensation processes in heat transfer Equipment*. Taylor & Francis.
- Cieśliński, J. T. and Krygier, K. A., 2014. "Sessile droplet contact angle of water-Al<sub>2</sub>O<sub>3</sub>, water-TiO<sub>2</sub> and water-Cu nanofluids". *Experimental Thermal and Fluid Science*, Vol. 59, pp. 258-263.
- Das, S. K.; Putra, N. and Roetzel, W., 2003. "Pool boiling of nano-fluids on horizontal narrow tubes". *International Journal of Multiphase Flow*, Vol. 29, No. 8, pp. 1237-1247.
- Giljean, S., Bigerelle, M., Anselme, K. and Haidara, H., 2011. "New insights on contact angle/roughness dependence on high surface energy materials". *Applied Surface Science*, Vol. 257, No. 22, pp. 9631-9638.
- Gu, H., Wang, C., Gong, S., Mei, Y., Li, H. and Ma, W., 2016. "Investigation on contact angle measurement methods and wettability transition of porous surfaces". *Surface and Coatings Technology*, Vol. 292, pp.72-77.
- Harish, G.; Emlin, V. and Sajith, V., 2011. "Effect of surface particle interactions during pool boiling of nanofluids." *International Journal of Thermal Sciences*, Vol. 50, No. 12, pp. 2318-2327.
- Kim, S. J.; Bang, I. C.; Buongiorno, J. and Hu, L. W., 2007. "Surface wettability change during pool boiling of nanofluids and its effect on critical heat flux". *International Journal of Heat and Mass Transfer*, Vol. 50, No. 19, pp. 4105-4116.
- Kwark, S. M.; Kumar, R.; Moreno, G.; Yoo, J. and You, S. M., 2010. "Pool boiling characteristics of low concentration nanofluids". *International Journal of Heat and Mass Transfer*, Vol. 53, No. 5, pp. 972-981.
- Kiyomura, I. S., Nascimento, F. J., Cunha, A. P. and Cardoso, E. M., 2015. "Analysis of the influence of surface roughness and nanoparticle concentration on the contact angle". In *Proceedings of 23rd ABCM International Congress of Mechanical Engineering (COBEM2015)*, Rio de Janeiro, Brazil.
- Massart, R., *Magnetic fluids and process for obtain them*. US Patent 4329241, 1982.

- Narayan, G. P.; Anoop, K. B. and Das, S. K., 2007. "Mechanism of enhancement/deterioration of boiling heat transfer using stable nanoparticle suspensions over vertical tubes". *Journal of Applied Physics*, Vol. 102, No. 7, p. 074317.
- Netto, F.P. Moraes, A.A.U. and Ribatski, G., 2013. "The effects of the nanoparticle concentration and surface roughness on the contact angle of nanofluids". In *Proceedings of 22nd ABCM International Congress of Mechanical Engineering (COBEM2013)*, Ribeirão Preto, Brazil.
- Raveshi, M. R., Keshavarz, A., Mojarrad, M. S. and Amiri, S., Experimental investigation of pool boiling heat transfer enhancement of alumina–water–ethylene glycol nanofluids. *Experimental Thermal and Fluid Science*, 44, pp. 805-814, 2013.
- Sarafraz, M. M. and Hormozi, F., 2014. "Nucleate pool boiling heat transfer characteristics of dilute Al<sub>2</sub>O<sub>3</sub>–ethyleneglycol nanofluids". *International Communications in Heat and Mass Transfer*, Vol. 58, pp. 96-104.
- Sarafraz, M.M., Hormozi, F. and Peyghambarzadeh, S.M., 2016. "Pool boiling heat transfer to aqueous alumina nanofluids on the plain and concentric circular micro-structured (CCM) surfaces". *Experimental Thermal and Fluid Science*, Vol. 72, pp. 125-139.
- Shahmoradi, Z.; Etesami, N. and Esfahany, M. N., 2013. "Pool boiling characteristics of nanofluid on flat plate based on heater surface analysis". *International Communications in Heat and Mass Transfer*, Vol. 47, pp. 113-120.
- Soltani, S.; Etemad, S. G. and Thibault, J., 2010. "Pool boiling heat transfer of non-Newtonian nanofluids". *International Communications in Heat and Mass Transfer*, Vol. 37, No. 1, pp. 29-33.
- Vafaei, S., 2015. "Nanofluid pool boiling heat transfer phenomenon". *Powder Technology*, Vol. 277, pp. 181-192.
- Wen, D., 2012. "Influence of nanoparticles on boiling heat transfer". *Applied Thermal Engineering*, Vol. 41, pp. 2-9.
- Wen, D. and Ding, Y., 2005. "Experimental investigation into the pool boiling heat transfer of aqueous based  $\gamma$ -alumina nanofluids". *Journal of Nanoparticle Research*, Vol. 7, No. 2-3, pp. 265-274.
- Zhang, F. and Jacobi, A. M., 2014. "Nanoparticle Deposition by Boiling on Aluminum Surfaces to Enhance Wettability". In *Proceedings of 15th International Refrigeration and Air Conditioning Conference*, West Lafayette, USA.

## 7. RESPONSIBILITY NOTICE

The authors are the only responsible for the printed material included in this paper.